Journal of Power Sources 196 (2011) 1750–1761

Contents lists available at ScienceDirect

Journal of Power Sources

journal homepage: www.elsevier.com/locate/jpowsour

Study of geometric stability and structural integrity of self-healing glass seal system used in solid oxide fuel cells

W.N. Liu*, X. Sun, M.A. Khaleel

Pacific Northwest National Laboratory, Richland, WA 99352, United States

ARTICLE INFO

Article history:
Received 23 July 2010
Received in revised form
30 September 2010
Accepted 1 October 2010
Available online 8 October 2010

Keywords:
Self-healing glass
SOFC
Geometry stability
Structure integrity
Creep
Modeling

ABSTRACT

A self-healing glass seal has the potential to restore its mechanical properties upon being reheated to the solid oxide fuel cell (SOFC) stack operating temperature. Such a self-healing feature is desirable for achieving high seal reliability during thermal cycling. Self-healing glass is also characterized by its low mechanical stiffness and high creep rate at SOFC operating temperatures. Therefore, the geometric stability and structural integrity of the glass seal system are critical to its successful application in SOFCs. This paper describes studies of the geometric stability and structural integrity of the self-healing glass seal system and the influence of various interfacial conditions during the operating and cooling-down processes using finite element analyses. For this purpose, the test cell used in the leakage tests for compliant glass seals, conducted at Pacific Northwest National Laboratory (PNNL), was taken as the initial modeling geometry. The effect of the ceramic stopper on the geometric stability of the self-healing glass sealants was studied first. Two interfacial conditions of the ceramic stopper and glass seals, i.e., bonded (strong) or unbonded (weak), were considered. Then the influences of interfacial strengths at various interfaces, i.e., stopper/glass, stopper/PEN, as well as stopper/IC plate, on the geometric stability and reliability of glass during the operating and cooling processes were examined.

1. Introduction

A renewed interest in the development of clean and efficient sources of power has been motivated by the volatility of the oil markets and the increasing concern with the environmental impact of noxious gas emissions. As an attractive power source, planar solid oxide fuel cells (SOFCs) are more efficient in energy conversion compared to the combustion of fossil fuels because energy conversion in a fuel cell is electrolytic, thereby eliminating harmful gas emissions. The successful development of such technology is, however, dependant on overcoming a series of technological hurdles. Planar SOFCs offer a significant advantage of a compact design along with higher power densities, but require incorporating hermetic gas seals for efficient and effective channeling of fuel and oxygen. Seals must adequately prevent the leakage of air and fuel, effectively isolate the fuel from the oxidant, and be electrically insulating [1,2].

As the most critical components in commercializing the planar SOFC technology, a lot of effort has been focused on the research and development of the sealing methods and sealant materials [3–5]. Mechanistically, there are two types of seals: compressive seals and rigid seals [6–8]. In compressive sealing, a compliant high-temperature material is captured between the two sealing surfaces and compressed with a load frame external to the stack to deliver hermetic sealing. The sealing surfaces can slide past one another without disrupting the hermeticity of the seal. This technology, however, remains incomplete because a reliable high-temperature sealing material is lacking [9], and it is difficult to design the load frame. Rigid seals rely on effective bonding of the seal material to the sealing surfaces. Rigid seals offer significant advantages over compressive seals, which suffer from problems of oxide scaling and chemical stability under highly reactive environments in addition to the disadvantage of incorporating an externally applied load by the appropriate load frame under high operating temperatures [10].

As rigid bonding, glass joining provides a cost-effective and relatively simple method of bonding ceramic and metal parts. Glass seals at room temperature are brittle, non-yielding, and particularly susceptible to fracture when exposed to tensile stresses. For this reason, in stack designs using glass seals, it is imperative that the temperature-dependent coefficients of thermal expansion (CTEs) for each of the joining components, i.e., the ceramic cell, the seal, and the metal separator, are approximately equal to minimize the buildup of residual stresses within the joint. Only a handful of high-temperature glass compositions in the borate- or phosphate-doped aluminosilicate families currently satisfy this requirement

* Corresponding author. Tel.: +1 509 372 4967; fax: +1 509 372 4672.
E-mail address: Wenning.Liu@pnl.gov (W.N. Liu).

0378-7753/$ – see front matter © 2010 Elsevier B.V. All rights reserved.
doi:10.1016/j.jpowsour.2010.10.002

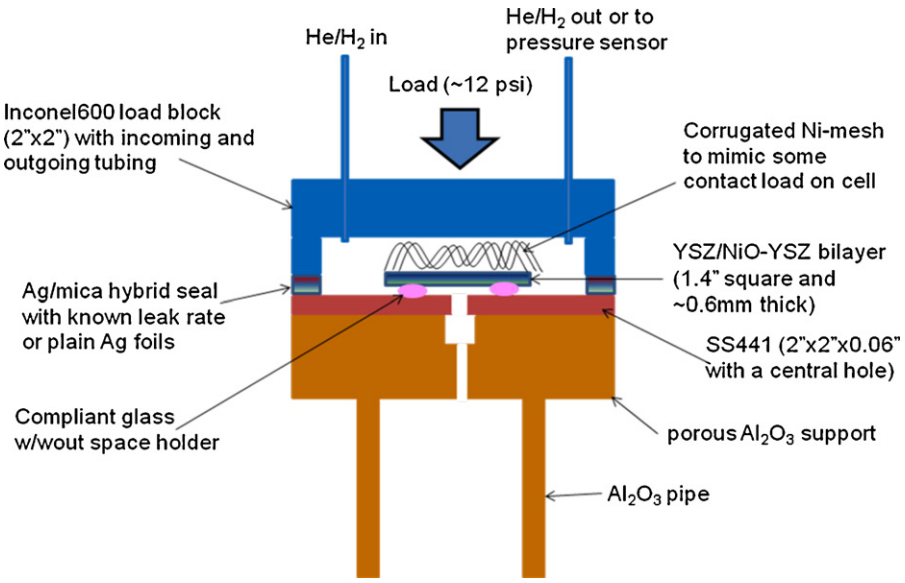

Fig. 1. Setup of leakage test [14].

[11]. However, it has to be noted that damaging the glass seals at the room temperature does not threaten the fuel cell stack because of lack of fuel and air at the shutdown stage. If the performance of the glass seal may be restored at the operating environments of SOFCs, the glass seal will be capable of being functional. Therefore, the concept of self-healing glass seals is emerging and attracting attention for sealants for SOFCs [12,13].

As its name implies, a self-healing glass seal has the potential to restore its mechanical properties upon being reheated to the stack operating temperature [12], even when it has experienced some cooling-induced damage/cracking at room temperature. Such a self-healing feature is desirable for achieving high seal reliability during thermal cycling. On the other hand, self-healing glass is also characterized by its low mechanical stiffness and high creep rate at the typical operating temperatures of SOFCs. When the glass reaches a temperature that exceeds the glass transition temperature (T_g), it will spread out under relatively small loads/pressures. When cooling down to room temperature, there is a potential for cracks and damage because of the CTE mismatch-induced residual stress. With a self-healing glass seal, therefore, the geometric stability and structural integrity of the sealing system become critical to its successful application in SOFCs. From a design perspective, it is important to know the long-term geometric stability and thermal mechanical behaviors of the self-healing glass under the stack operating conditions.

This paper describes studies regarding the geometric stability of self-healing glass and the influence of various interfacial conditions of ceramic stoppers with the positive electrode–electrolyte–negative electrode (PEN), interconnect (IC), and glass seal. The studies were done with finite element analysis. The structural integrity of the glass seal was examined during the operating and cooling-down processes. For this purpose, the test cell used in the leakage tests with compliant glass seals, conducted at PNNL, was taken as the initial modeling geometry.

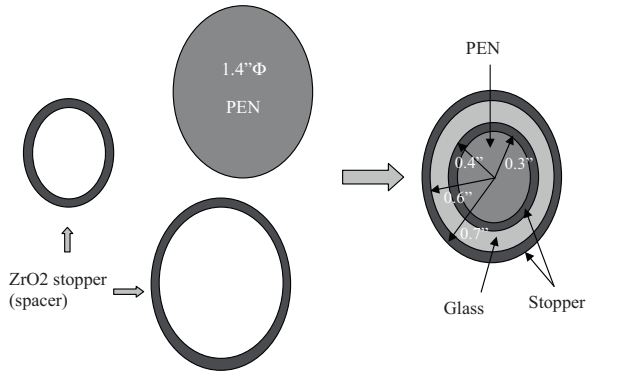

Fig. 2. Geometry of PEN, ceramic stopper, and seal in the test cell.

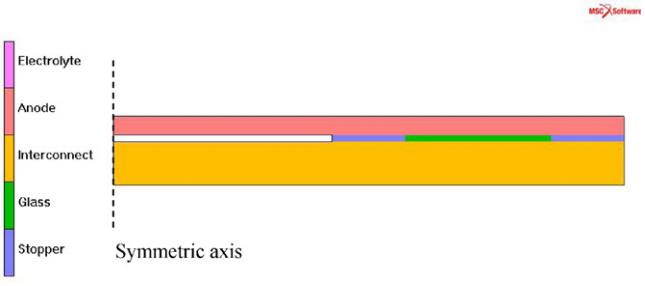

Fig. 3. Numerical model.

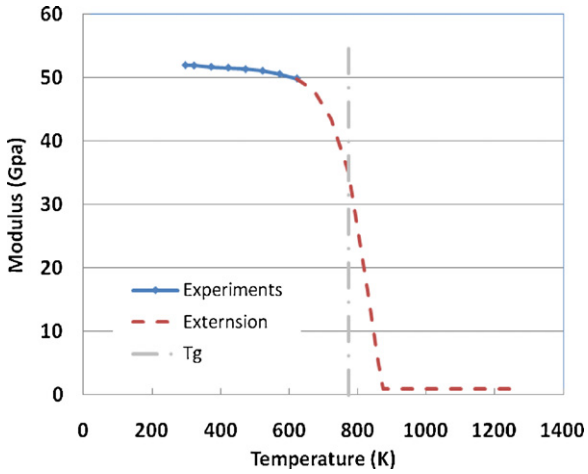

Fig. 4. Temperature dependent Young's modulus of SCN glass [15].

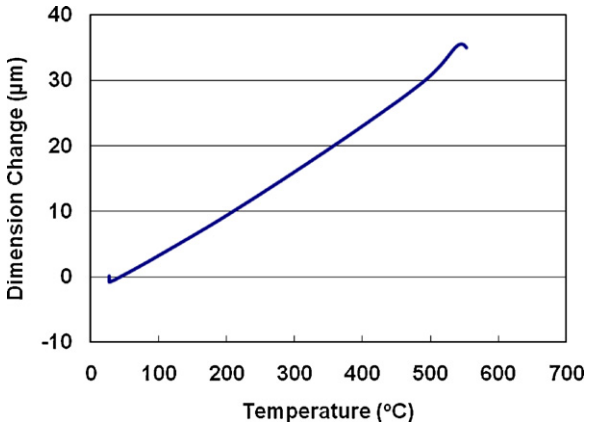

Fig. 5. Dimension change of specimen of SCN-1 glass in CTE test [18].

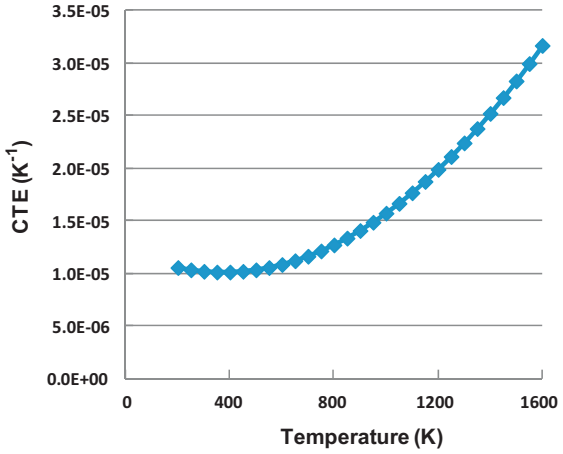

Fig. 6. Temperature dependent CTE of glass [19].

The effect of the ceramic stopper on the geometric stability of the self-healing glass sealants was studied first. Two interfacial conditions of the ceramic stopper and glass seals, i.e., bonded (strong) or unbonded (weak), were considered. Then the influences of interfacial strengths at various interfaces, i.e., stopper/glass and stopper/PEN as well as stopper/IC plate, on the geometric stability and reliability of glass during the operating and cooling processes were examined.

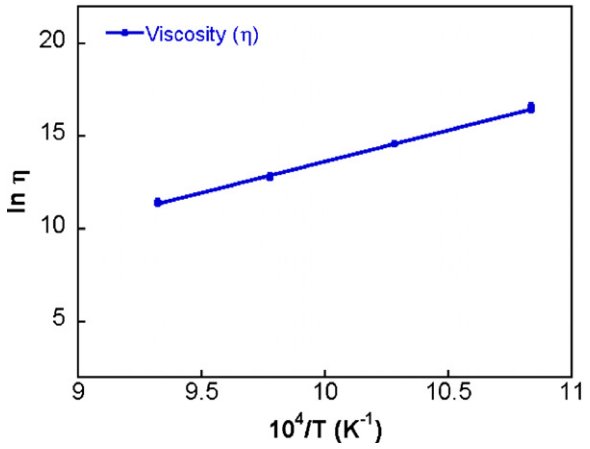

Fig. 8. Creep behavior of the SCN-1 glass [20].

2. Setup and geometry of test cell

The leakage tests were conducted at Pacific Northwest National Laboratory. The test cell used in the leakage tests with compliant glass seals was used as the initial modeling geometry. Fig. 1 shows the set up of the test cell [14]. The core part of the setup consisted of compliant glass with/without space holder, YSZ/NiO–YSZ bilayer, and SS441 interconnect. The associated seal geometry of the test cell is depicted in Fig. 2.

To simulate the glass behavior in the test, only the core part of the setup in Fig. 1 was taken into account, which includes PEN, stopper/glass, and IC plate. Fig. 3 shows the computational cross-section of the test cell. Due to the symmetrical nature of the test cell geometry, a 2-dimensional axisymmetric model was used in this study. The numerical model included the anode/electrolyte PEN, the inner/outer ceramic stoppers, the glass seal, and the SS441 interconnect.

3. Mechanical property of materials and finite element model

In the present paper, glass SCN-1 was used as the pure glass seal in the test cell modeling. Its thermal and mechanical properties are temperature-dependent. Fig. 4 depicts the temperature-dependent Young's modulus, partially measured experimentally by Oak Ridge National Laboratory (ORNL) [15]. It may be seen that the measurement was only conducted up to the glass transition temperature,

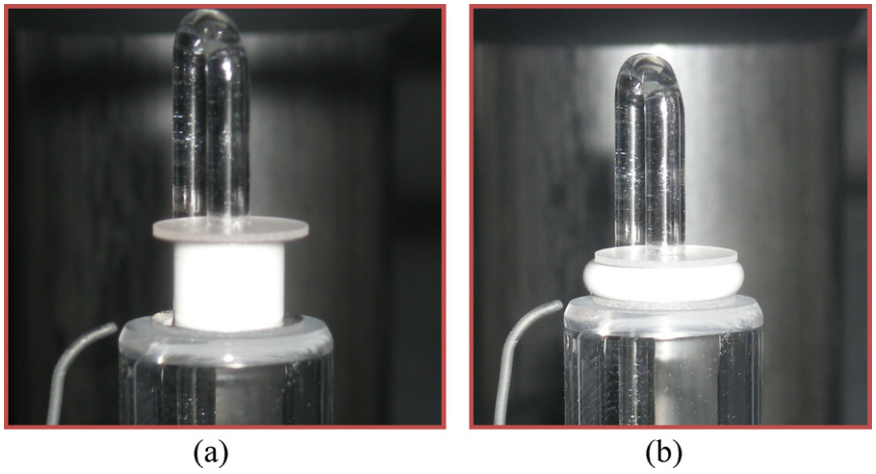

Fig. 7. Setup of viscosity measurement with TMA. (a) before viscosity measurement; (b) after viscosity measurement [20].

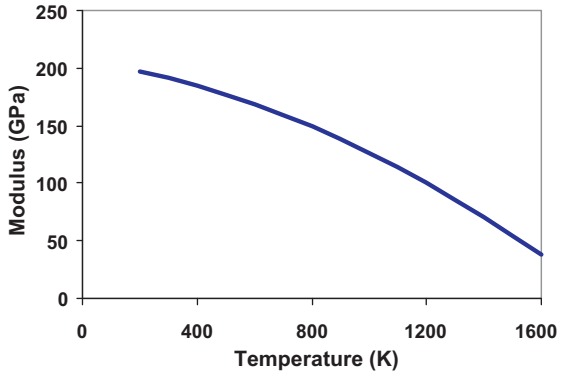

Fig. 9. Temperature-dependent Young's modulus of SS441.

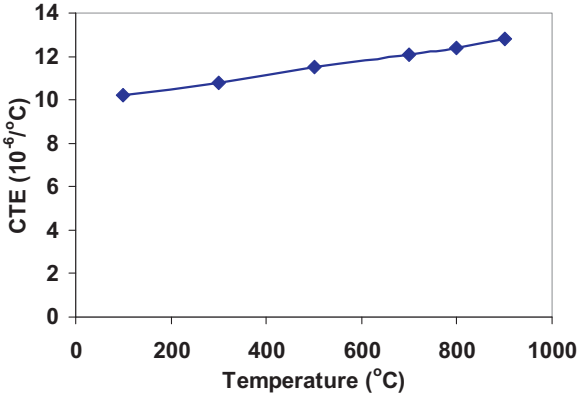

Fig. 10. Temperature-dependent CTE of SS441.

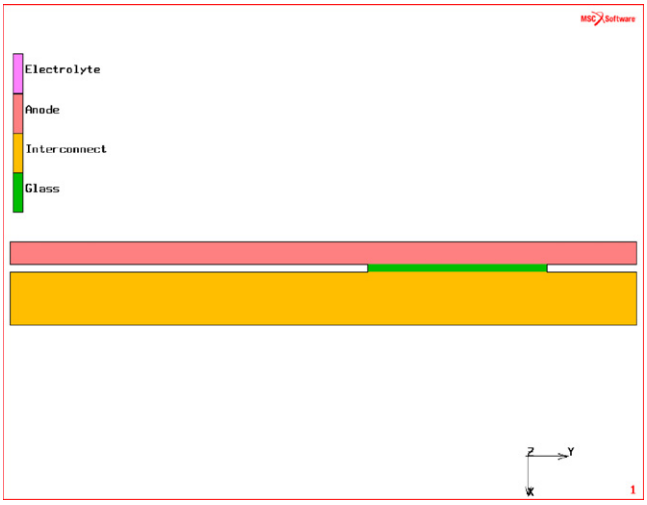

Fig. 12. Schematic of model of setup without ceramic stoppers.

i.e., the T_g of this glass. This is because the testing method is no longer valid when the temperature exceeds T_g. In this analysis, the high-temperature modulus was extrapolated in a manner consistent with typical glass behavior [16,17].

The glass transition temperature, T_g, of SCN-1 is about 500 °C, which is substantially lower than the typical operating temperature of SOFCs (~800 °C). The measured CTE for SCN-1 [18] is available only up to about 600 °C because of the limit of its T_g (see Fig. 5), so temperature dependent CTE data from the literature [19] shown in Fig. 6 were used in the current simulation for temperatures greater than 600 °C.

At the typical operating temperature of an SOFC, the creep behavior of the pure glass is unavoidable. Its creep behavior at high

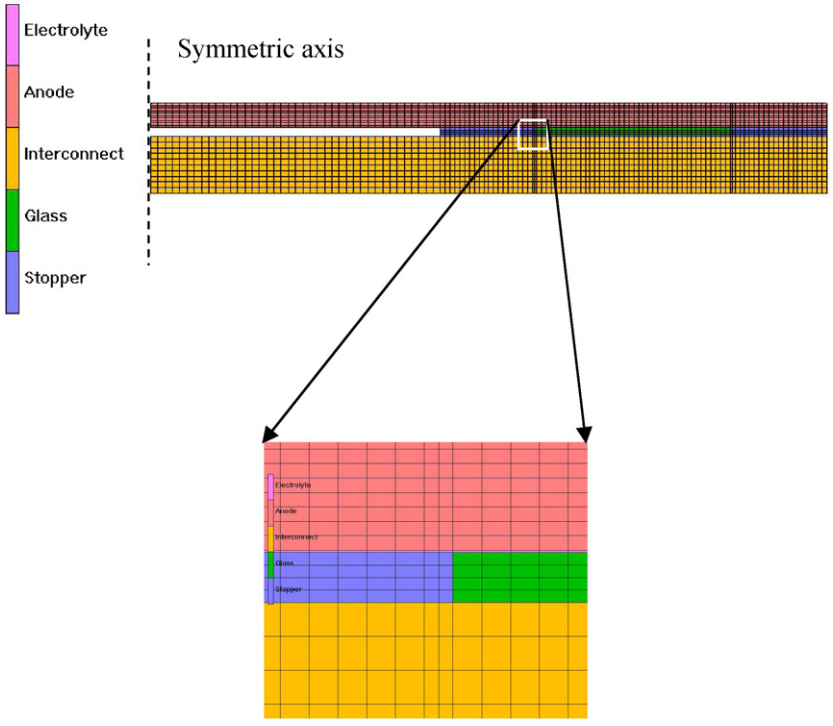

Fig. 11. FE mesh used in the simulation.

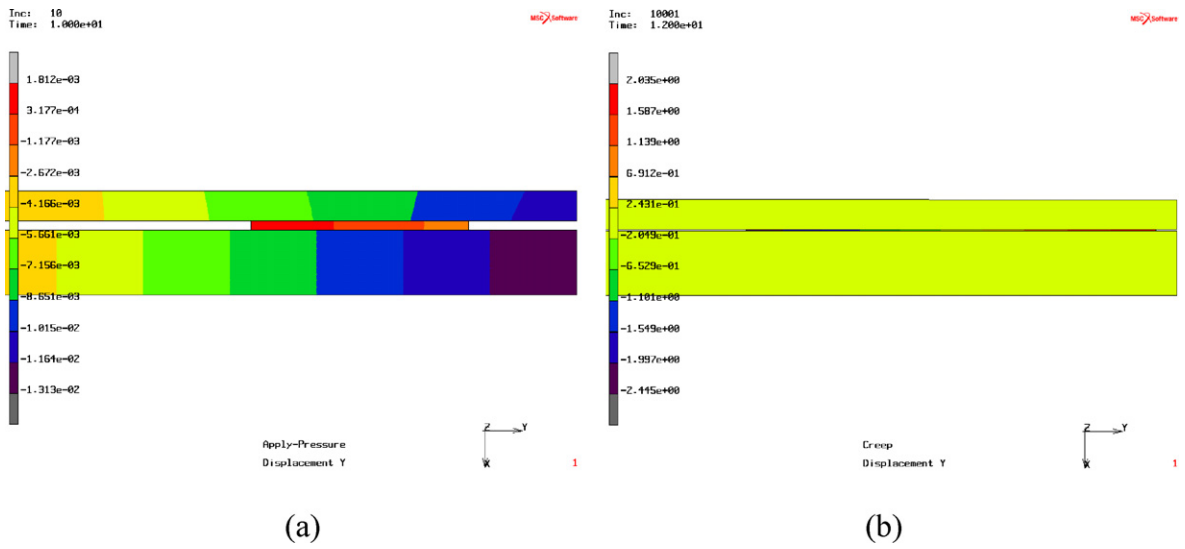

Fig. 13. Deformed configurations (a) after applying top pressure; (b) creep in 2 s.

temperature was measured at ORNL with the setup shown in Fig. 7. The measurements were performed isothermally at temperatures between 600 °C and 850 °C. Three different loads were used in the viscosity measurement. A constant heating rate of 5 °C/min was applied under a constant load [20].

Viscous behavior of the pure glass can be evaluated by the linear creep law as [20]:

$$\dot{\varepsilon} = \frac{1}{\eta}\sigma \tag{1}$$

where $\eta = \eta_0 \exp(Q_V/RT)$, and R is the universal gas constant with a value of 8.314 J K^{-1} mol^{-1}. Based on the measurement results, the parameters for SNC-1 self-healing glass can be determined as $\eta_0 = 1.397 \times 10^{-9}$ Pa s, and $Q_v = 283.32$ kJ mol^{-1} [20]. The viscous parameter η of the self-healing glass is plotted as a function of temperature in Fig. 8.

The mechanical property of SS441 used as the interconnect here is also temperature-dependent. The mechanical properties of SS441 are depicted in Figs. 9 and 10 for Young's modulus and CTE, respectively [21,22]. As pointed out in [23], creep deformation becomes relevant for a material when the operating temperature exceeds or even is less than half of its melting temperature (in degrees of Kelvin). The operating temperatures for most of the SOFCs under development are around 1073 K. Considering that the

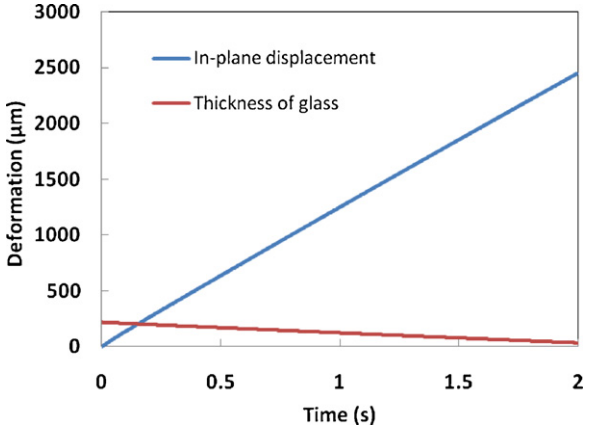

Fig. 14. Deformation history of the inner side of the glass.

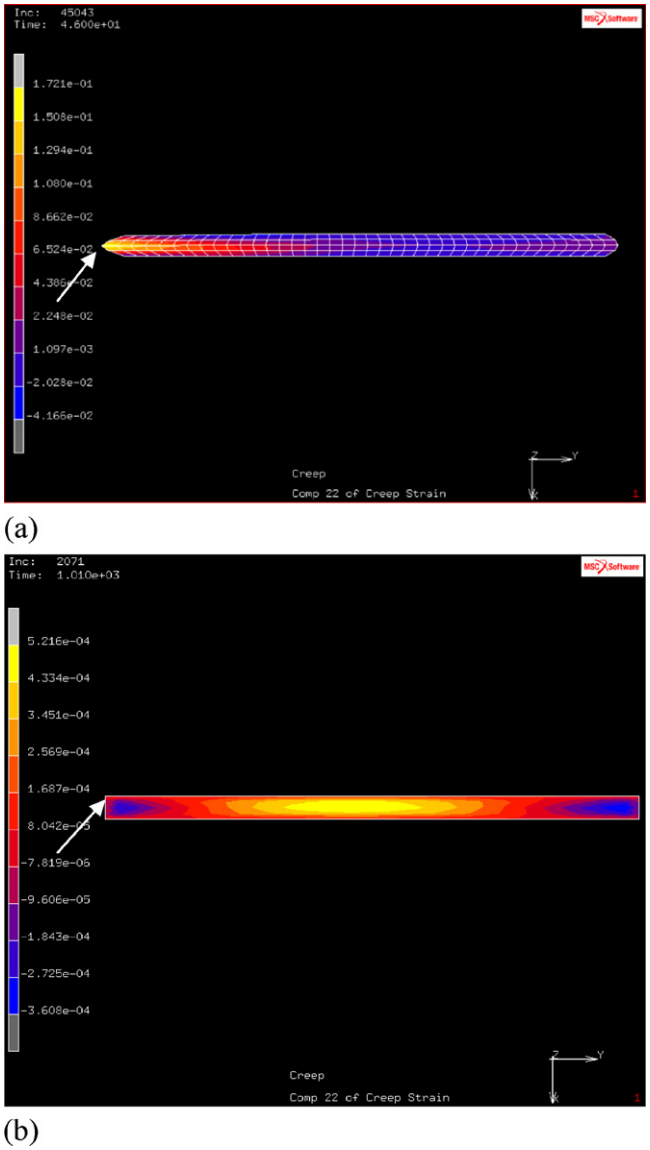

Fig. 15. Deformed glass with distribution of equivalent creep strain after creep. (a) 36 s of creep without stopper; (b) 1000 s of creep with ceramic stopper.

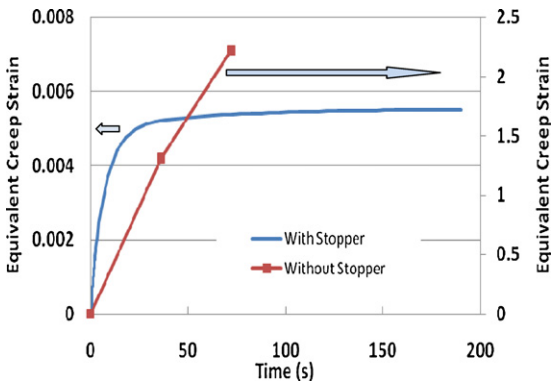

Fig. 16. History of equivalent creep strain.

melting temperature for most stainless steel (SS) is approximately 1800 K, the possible creep deformation of ferritic IC under the typical cell operating temperature should not be neglected. However, compared with the creep behavior of the glass SCN-1, the creep strain rate of the high-temperature stainless steel [24] is lower than that of glass SCN-1 by six orders of magnitude; therefore, the creep behavior of SS441 is neglected here.

The simulation was performed using the commercial finite element (FE) software package MARC [25]. Fig. 11 shows the FE mesh used in the simulation with details around the seal, PEN, and IC interface area. Two types of sealing systems are considered: 100% glass seals and glass seals with ceramic stopper rings at both inner and outer radii of the glass seal; see Fig. 11.

The initial stress-free temperature was assumed to be the stack assembly temperature of 850 °C. The operating temperature is 800 °C. The test cell was given the initial stress-free temperature and then dropped to the operating temperature in a quasi-static analysis step. The CTE mismatch among various components will lead to various degrees of thermal stresses in different components due to the temperature drop. However, at the constant stack operating temperature, the glass seal will creep under the thermal stress, resulting in stress relaxation and redistribution. Upon shutdown of the test cell and cooling down to the room temperature of 25 °C, new thermal stresses will be created because of the CTE mismatch. The glass seal stress and the interfacial stress distributions at different stages of the thermal profile described above will be presented to compare the effects of these different sealing systems.

4. Results and discussions of the parametric study

To explore the performance of the self-healing glass in SOFC stacks, different design and interfacial conditions were considered. At first, the behavior of the glass was studied without and with

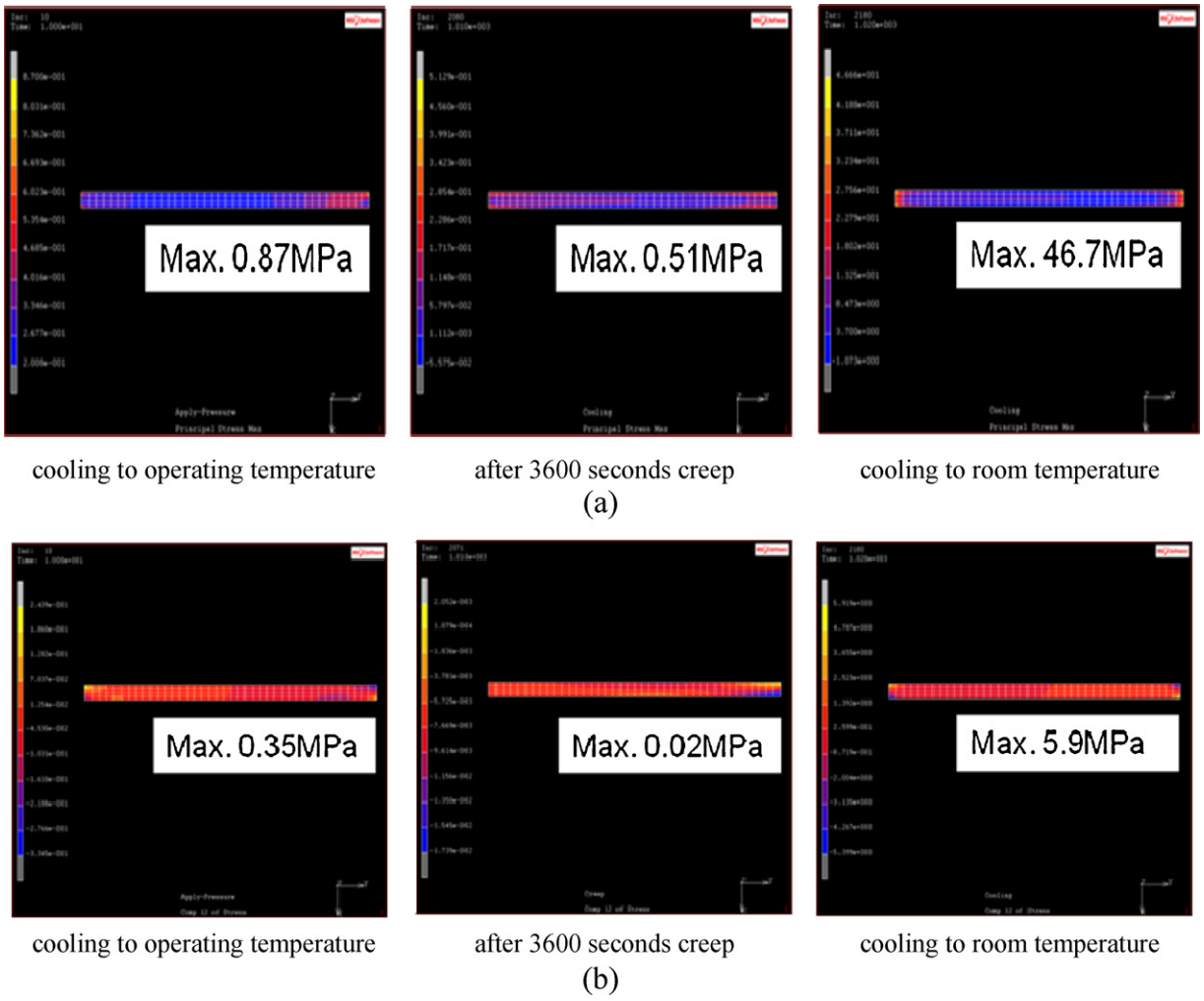

Fig. 17. Stress contour of glass seal at the different time: weak interface between stopper and glass seal, (a) maximum principal stress; (b) shear stress S12.

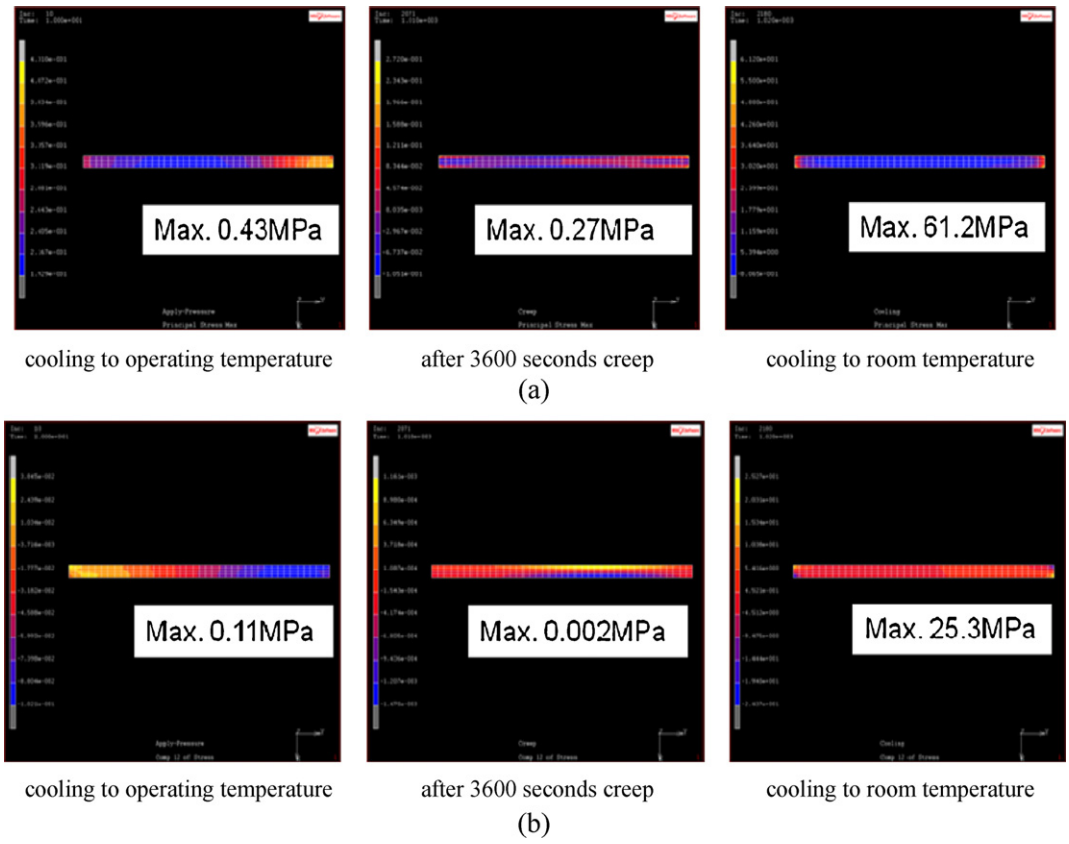

Fig. 18. Stress contour of glass seal at the different time: strong interface of stopper and glass seal, (a) maximum principal stress; (b) shear stress S12.

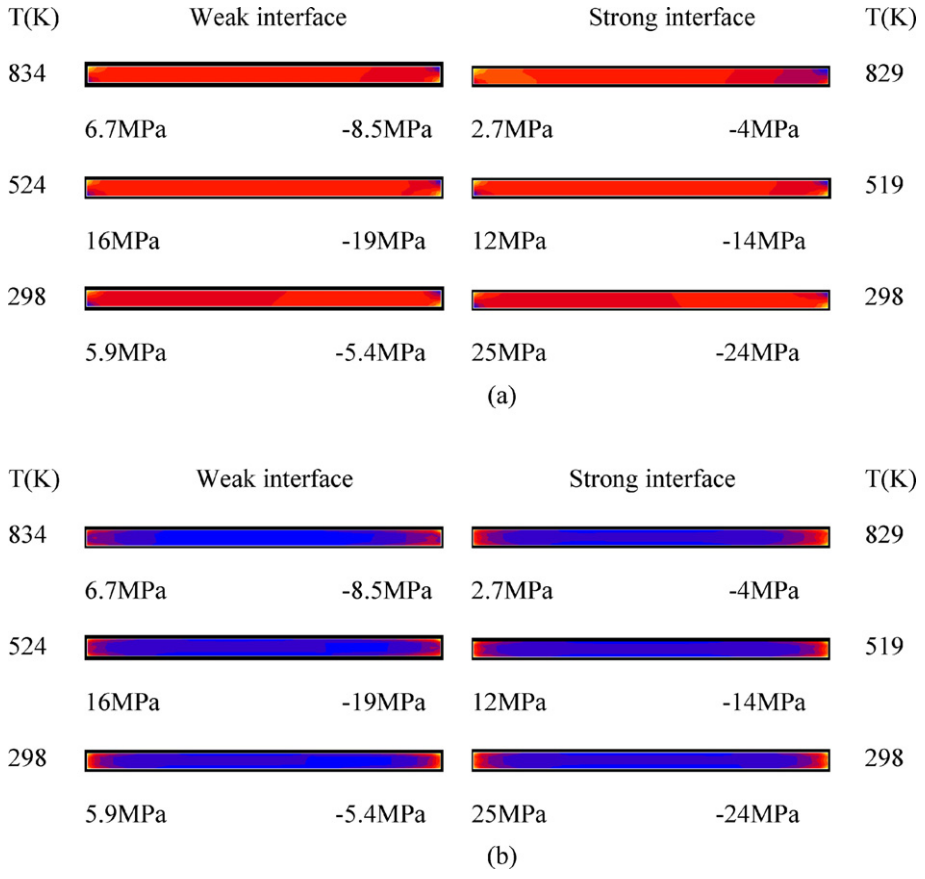

Fig. 19. Stress distribution during the shutdown process with a weak and a strong interface of the stopper and the glass: (a) shear stress; (b) normal stress.

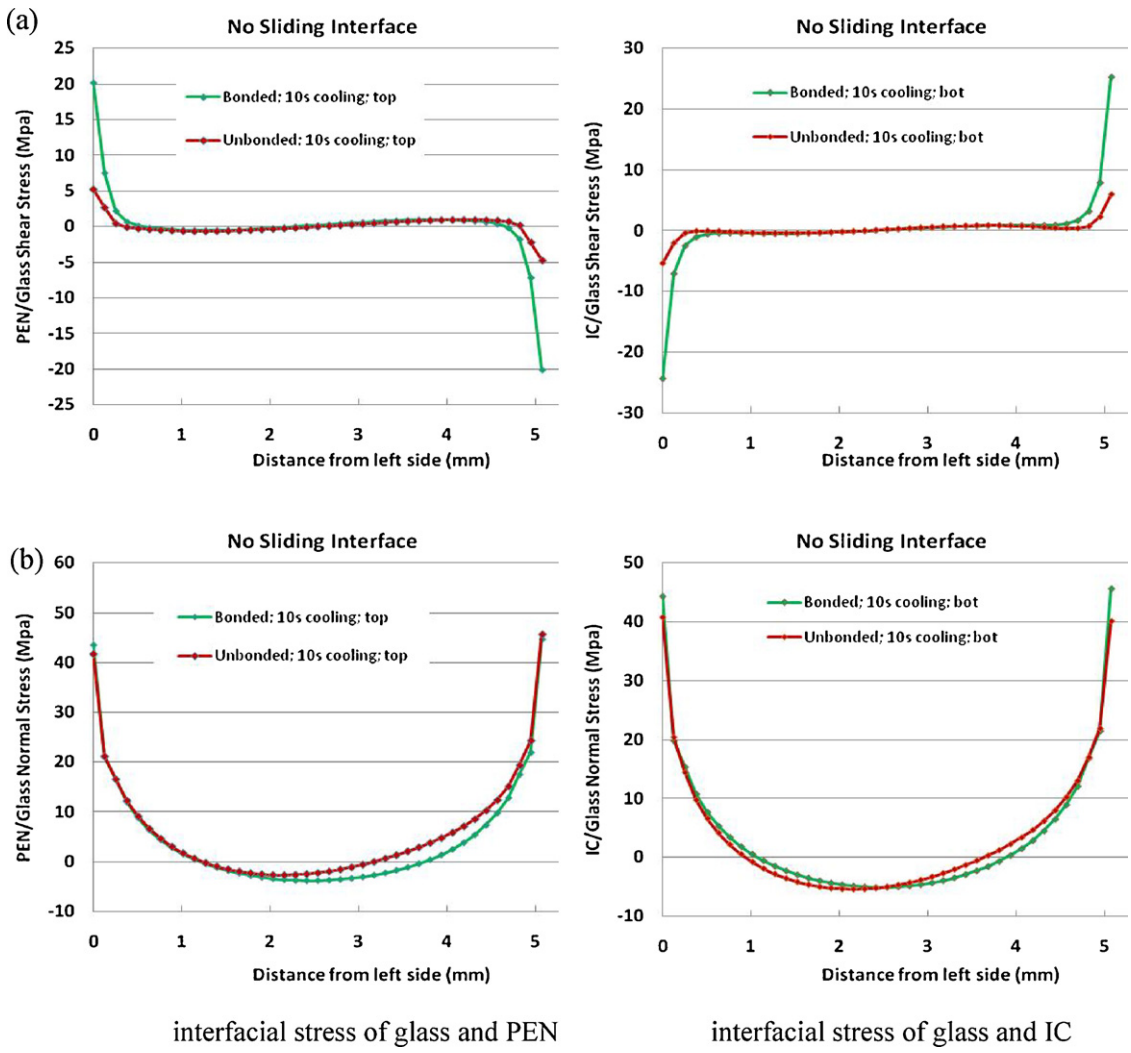

Fig. 20. No sliding interface between the stopper and PEN/IC with the interface of the stopper and the glass: (a) weak (unbonded); (b) strong (bonded).

ceramic stoppers. Then, the effect of viscosity of the glass at high temperature on the stress in the glass was studied using creep analysis. Subsequently, the interfacial conditions in the ceramic stopper/glass and stopper/PEN as well as stopper/IC plate interfaces were investigated at two extreme conditions: fully bonded and sliding. For the stopper and glass interface, two cases were considered, one with a gap of 0.0635 mm between the stopper and glass seal and one with no gap between them.

4.1. Geometric stability of the glass seal

In the first case, a pure SCN-1 glass seal was applied without the ceramic stoppers at its inner and outer radii; see Fig. 12. A constant pressure of 0.08 MPa was applied on the top surface of PEN. The glass was allowed to flow freely along the interfaces with the PEN and IC plate. The deformed configurations immediately after the pressure application and after 2 s of creep deformation are illustrated in Fig. 13, respectively. Immediately after the application of the top pressure, the glass still kept its original geometry. However, the glass was predicted to flow quickly with time in the creep analysis. The final thickness of the glass was almost invisible. Fig. 14 shows the history of deformation of the left side, i.e., the inner radius, of the glass. The in-plane deformation increased almost linearly, and the thickness of the glass decreased in the same linear manner. That means that the glass will quickly flow out between the PEN and IC plate if no physical containment is established at the PEN and IC.

Subsequently, another case was considered where the glass was not allowed to flow along the interfaces with PEN and IC. To compare the influence of the ceramic stopper, the results with and without the ceramic stoppers are discussed here. Fig. 15 shows the deformed geometry of the glass without and with the stopper. Fig. 15(a) shows the deformed configuration of the glass seal after 36 s of creep for the sealing system with 100% glass seal and no ceramic stopper. Fig. 15(b) shows the deformed configuration of the glass seal after 1000 s of creep for the sealing system with 100% glass seal but with ceramic stopper. At the constrained points along the interfaces with PEN and IC, the glass material cannot move along the interfaces; however, the glass at the middle part away from the interface will still flow out. The equivalent creep strain history at the middle point of the left edge over time [marked by an arrow in Fig. 15(a) and (b)] is depicted in Fig. 16. It is obvious that without the ceramic stopper, the strain at the middle part of the glass will continue to linearly increase. Such a linear strain versus time indicates that the 100% glass seal will continue to flow over time. With the ceramic stopper, the creep deformation occurs only at the initial stage and then remains constant because the shear stress in the glass will be relaxed out quickly and transferred into the ceramic stopper. Therefore, the geometry of the glass will be kept intact by the ceramic stopper.

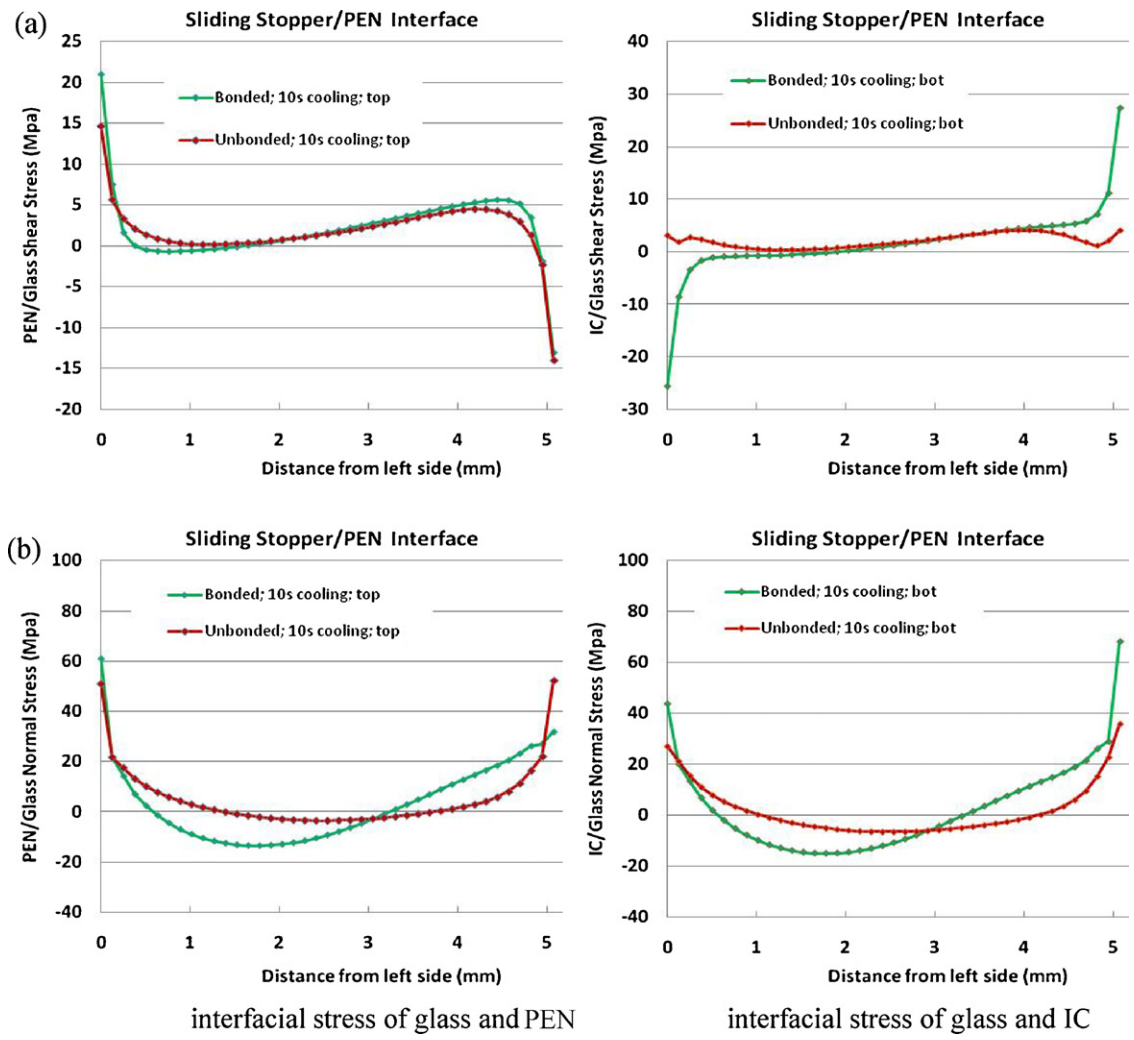

Fig. 21. Sliding interface between stopper and PEN with interface of stopper and glass: (a) weak (unbonded); (b) strong (bonded).

4.2. Stresses in the glass seal

To prevent the glass seal out-flow, inner and outer ceramic stopper rings like those illustrated in Figs. 2 and 3 were added to the next sealing system. Note that the glass seal and the ceramic stoppers were not bonded, and a small numerical gap of 0.063 mm was present in the model. Fig. 17 shows the distribution of maximum principal stress and shear stress in the glass seal at different stages of the simulation. Upon the initial temperature drop from the stress-free temperature to the SOFC operating temperature, small magnitudes of thermal stresses were induced in the glass seal. These stresses were relaxed out to even lower values during the first 3600 s of cell operation because of the creep behaviors of the glass seal. Upon cooling down to room temperature, relatively high thermal stress is predicted. These modeling results indicate that the final cooling step to room temperature is the most aggressive one in terms of creating high stresses in the glass seal and is most likely to create some degree of damage in the glass seal. The exact degree of damage would depend on the bulk strength of the glass seal at room temperature. However, if the glass seal is truly self-healing, then the cracks/damages will be closed/healed upon reheating to the stack operating temperature, and the whole process will repeat itself during the next thermal cycle.

For the next sealing system design, the case where the ceramic stopper and the glass seal are fully bonded was examined. Fig. 18 illustrates the modeling results of the maximum principal stress and shear stress in the glass seal at different time steps, respectively. The trend in the stress history in the seal was similar to those presented earlier with a gap. However, in this case, the magnitudes of the tensile and shear stress upon cooling to room temperature were much higher than those predicted earlier for the unbonded case with a small gap. These results indicate that leaving a small physical gap between the glass and ceramic seal will help mitigate cooling-induced stress buildup in the seal, therefore reducing the degree of damage the glass seal may have upon cooling. Again, if the glass seal is truly self-healing, the magnitude of room temperature damage may not matter because all of the cracks will be closed up and healed upon the next operating cycle.

Fig. 19 depicts the distribution of the shear stress and normal stress in the glass, respectively, during the cooling-down process with a bonded (strong) or bonded (weak) interface of stopper and glass. In Fig. 19, with the weak interface of stopper and glass, the stress in the glass was mainly related to the CTE mismatch between the glass, PEN, and IC. The temperature-dependent CTE curves of glass and PEN intersect at the intermediate temperature of about 600 K; i.e., the CTE of glass is higher than that of PEN at high temperatures, but lower than that of PEN at lower temperatures. With the strong interface of stopper and glass, the stress in the glass, particularly near the interface, is influenced by the ceramic properties. After the cooling-down process, the weak interface of the stopper and glass will create less interfacial shear stress and similar normal tensile stress. Whether the interface of the ceramic stopper

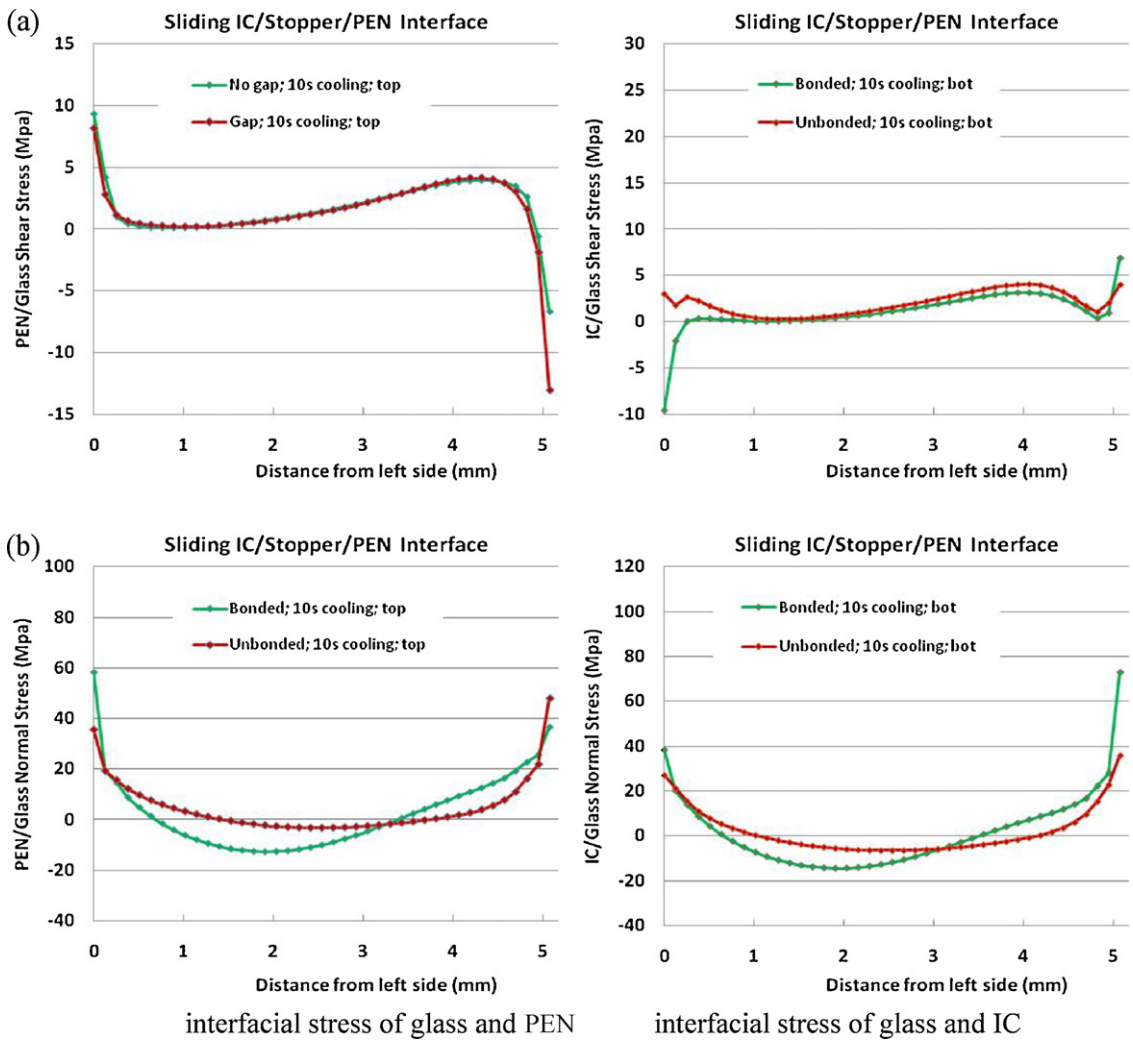

Fig. 22. Sliding interface between stopper and PEN/IC with interface of stopper and glass: (a) weak (unbonded); (b) strong (bonded).

and glass is strong or not, the highest stresses always occur at the edge of glass. In Fig. 19, both of the maximum and minimum values of the stresses are given. For shear stresses, the positive and negative signs represent the directions of the shear stress; therefore, only their magnitude has physical significance. For normal stresses, however, a positive value represents tensile normal stress on the interface, while a negative value represents compressive normal stress. Only a tensile normal stress on the interface will promote opening of the interface, i.e., interface delamination. Even though the maximum principal stress and he shear stress with the weak interface of the stopper and glass are slightly larger than those with the strong interface of the stopper and glass, these stresses with the weak interface of the stopper and glass are much less that those with the strong interface of the stopper and glass. That means that when the self-healing glass system is designed, there is no need to be concerned about the interfacial adhesion of the stopper and glass. The weak interface of the stopper and glass will help to reduce the stress level in glass seals.

4.3. Effect of interfacial conditions of stopper with other components

When applying ceramic stoppers to prevent the out-flow of the glass, the interfacial properties of the ceramic stopper with other components such as PEN, IC, and glass are closely dependent on the ceramic material and processing parameters. To evaluate the effect of the interfacial behaviors of the ceramic stopper with the PEN and IC plate on the structure stability of the cell, two extreme cases – bonded and sliding – are considered here for bounding purposes. For any boundary conditions of the stopper with the PEN and the IC, two types of interfaces between the stopper and glass are always considered here: bonded and unbonded.

Figs. 20–22 show the normal and shear stress distributions along the interfaces of glass with PEN and IC over the distance that starts from the innermost ends of the interfaces for the different interface conditions of the ceramic stoppers and PEN/IC, respectively. For Fig. 20, the interfaces between the ceramic stoppers and PEN/IC are bonded. The predicted results show that the interfacial shear and normal stresses have a high level only near the edges. The interfacial shear stress near the edge with the unbonded interface of the stopper and the glass is much less than that with the bonded interface of the stopper and the glass. Though the bonded interface of the stopper and the glass leads to higher interfacial normal stress, the influence of the interface of the stopper and the glass on the interfacial normal stress is negligible. For Fig. 21, the interface conditions of the stoppers with the PEN and the IC are different: sliding with the PEN but bonded with the IC. In this case, the interfacial shear stresses on the interfaces of the glass with the PEN and the IC are different. On the interface of the glass and the PEN, the interfacial shear stress has a high level near the edges of the glass regardless

of the condition of the interface of the stoppers and the glass. The influence of the interface of the stoppers and glass is negligible. For the interface of the glass and IC, however, the effect of the interface condition of the stoppers and the glass are significant: the bonded interface of the stoppers and the glass results in much higher stress near the edge of the glass. The interfacial normal stresses on the interfaces of the glass with the PEN and IC are similar. The interfacial conditions of the stoppers and glass have some influence on the distribution of the interfacial normal stress of the interfaces of the glass with the PEN and IC: the unbonded interface of the stopper and the glass leads to uniform distribution of the interfacial normal stress except the edge of the glass. Also, the bonded interface of the stoppers and glass leads to compressive normal stress on the inner half part of the interface of the glass with the PEN and IC and to tensile normal stress on the outer half part of the interface of the glass with the PEN and IC. With the sliding interfaces of the stoppers with the PEN and IC as shown in Fig. 22, the interfacial shear and normal stresses are similar to those as shown in Fig. 21; i.e., sliding interface of the stopper and the PEN and the bonded interface of the stopper and IC. That means that the interfacial condition of the ceramic stopper and IC does not influence the interfacial shear and normal stresses on the interface of the glass with the PEN and IC.

Regardless of the interface properties between the ceramic stopper and PEN/IC, the weak interface between the stopper and glass will always create a lower interfacial shear stress on both the glass/PEN and the glass/IC interfaces. The effect of the interfacial condition of the stopper and glass on the interfacial normal stress is less than that on the interfacial shear stress. In any case, high interfacial shear stress and normal stress are predicted in the vicinity of the two edges of the glass seal. The maximum normal stress on the interface is always higher than the maximum shear stress on the interface. The high interfacial normal stresses at the edge of the glass may lead to localized failure of the glass seal at the edge after cooling down to room temperature. It may also be seen that the normal stresses on the interfaces of glass with the PEN and IC remain compressive in the middle portion of the glass seal; therefore, the structural integrity of the glass seals will be maintained even if some localized edge failures occur during cooling.

5. Conclusions

This paper discusses studies of the geometric stability of self-healing glass and the influence of various interfacial conditions of ceramic stoppers with the PEN, IC, and glass seal on the structural integrity of the glass seal during the operating and cooling-down processes. The studies were done with finite element analysis. Two interfacial conditions of the ceramic stopper and glass seals, i.e., bonded (strong) or unbonded (weak), are considered. The interfacial conditions of the ceramic stopper with the PEN and IC plates are assumed to be bonded or sliding. Based on the analyses results, the following observations and conclusions can be made:

(1) Self-healing glass alone cannot sustain its geometry in a sealing system for SOFC. The glass seal material will flow out quickly because of its low viscosity at a high SOFC operating temperature.
(2) Ceramic stoppers are necessary and helpful in maintaining the geometric stability of the self-healing glass in a sealing system for SOFCs.
(3) Under the operating environment of SOFCs, the stress level in the glass seal is very low. The initial stresses induced by the temperature drop from the stress-free assembly temperature to the working temperature of SOFCs are relaxed quickly during the operation of SOFCs.
(4) After the cooling-down process, the CTE mismatch will result in relatively high stress in glass materials and on the interfaces of the glass seal with other components. It should be noted that the high stress occurs only locally at the edges of the glass seal, which may cause localized failure of the glass interfaces.
(5) Despite the localized tensile normal stress at the interface between the glass seal with the PEN and IC, the compressive normal stresses in the middle portion of the glass seal will maintain the structural integrity of the glass seal system.

In this paper, the volume change induced by sintering of the glass is not considered. Possible volume changes of the glass during the sintering process and their influence on the structural integrity of the sealing system in SOFCs is important for designing the glass seal system. The effects of the applied glass paste volume and the ceramic stoppers geometry as well as the thermal–mechanical properties of glass on the geometric stability and structural integrity of the glass seal system will be studied in the following work.

Acknowledgements

Pacific Northwest National Laboratory is operated for the U.S. Department of Energy by Battelle under Contract DE-AC05-76RL01830. The work summarized in this report was funded as part of the Solid-State Energy Conversion Alliance Core Technology Program by the U.S. Department of Energy's National Energy Technology Laboratory. We would like to acknowledge the technical direction from Travis Shultz and Briggs White. Technical discussions with Drs. Matt Chou and Jeff Stevenson are also gratefully acknowledged.

References

[1] R.N. Singh, Journal of Materials Engineering and Performance 15 (4) (2006) 422–426.
[2] W.N. Liu, X. Sun, M.A. Khaleel, Journal of Power Sources 185 (2) (2008) 1193–1200.
[3] K.A Nielsen, M. Solvang, S.B.L. Nielsen, A.R. Dinesen, D. Beeaff, P.H. Larsen, Journal of the European Ceramic Society 27 (2–3) (2007) 1817–1822.
[4] S.R. Choi, N.P. Bansal, Ceramic Engineering and Science Proceedings 26 (4) (2005) 275–283.
[5] F. Smeacetto, M. Salvo, M. Ferraris, J. Cho, A.R. Boccaccini, Journal of the European Ceramic Society 28 (1) (2008) 61–68.
[6] R.N. Singh, Ceramic Engineering and Science Proceedings 26 (4) (2005) 247–255.
[7] J.W. Fergus, Journal of Power Sources 147 (1–2) (2005) 46–57.
[8] Y.S. Chou, J.W. Stevenson, L.A. Chick, Journal of America Ceramic Society 86 (6) (2003) 1003–1007.
[9] S.B. Sang, W. Li, J. Pu, L. Jian, Journal of Power Sources 177 (1) (2008) 77–82.
[10] S.P. Simner, J.W. Stevenson, Journal of Power Sources 102 (1–2) (2001) 310–316.
[11] N. Lahl, L. Singheiser, K. Hilpert, K. Singh, D. Bahadur, Proceedings of the Sixth International Symposium on Solid Oxide Fuel Cells, The Electrochemical Society, Pennington, NJ, 1999, pp. 1057–1065.
[12] W.N. Liu, X. Sun, B. Koeppel, M. Khaleel, International Journal of Applied Ceramic Technology 7 (1) (2010) 22–29.
[13] R.N. Singh, International Journal of Applied Ceramic Technology 4 (2) (2007) 134–144.
[14] Y.S. Chou, E. Mast, E. Thompson, J.W. Stevenson, Compliant Glass Seal Development, NETL Review Meeting, Richland, WA, USA, November 03, 2009.
[15] E. Lara-Curzio, A. Shyam, R.M. Trejo, Y.L. Wang, Characterization of SCN-1 glass, Technical Report, Oak Ridge National Laboratory, 2009.
[16] E.L. Bourhis, P. Gadaud, J.P. Guin, N. Tournerie, X.H. Zhang, J. Lucas, T. Rouxel, Scripta Materilia 45 (2001) 317–323.
[17] J.P. Andrews, Proceedings of the Physical Society of London 37 (1924) 169–177.
[18] E. Lara-Curzio, A. Shyam, R.M. Trejo, Y.L. Wang, Internal Communication (March 2010).
[19] N. Govindaraju, W.N. Liu, X. Sun, P. Singh, R.N. Singh, Journal of Power Sources 190 (2) (2009) 476–484.
[20] R.M. Trejo, Y. Wang, A. Sides, A. Shyam, E. Lara-Curzio, Viscosity and Wetting Behavior of SCN-1 Glass, NETL Review Meeting, Internal Communication, Richland, WA, November 2009.

[21] Product Data Bulletin, 441 Stainless Steel, UNS S44100 Preliminary Bulletin, AK Steel. http://www.aksteel.com/pdf/markets_products/Stainless/ferritic/441_Data_Bulletin.pdf, 2007.
[22] Technical Data Blue Sheet, Stainless Steel AL 441HP Alloy, ATI Allegheny Ludlum. http://www.alleghenyludlum.com/ludlum/documents/441.pdf, 2005.
[23] W.N. Liu, X. Sun, M.A. Khaleel, Fuel Cells 10 (4) (2010) 703–717.
[24] R.C. Lobb, R.B. Jones, Journal of Nuclear Materials 91 (2–3) (1980) 257–264.
[25] MARC, Version 2007r1. http://www.mscsoftware.com/products/marc.cfm?Q=131&Z=396&Y=400, 2007.